ART & TECHNOLOGY PUBLISHING PTE. LTD.

Progress in Human Computer Interaction

2022 Volume 2, Issue 1

ISSN: 2630-4635

A Study on the Performance Analysis of the Dual-Arm Robot for the Assembly Task

Gi-Hoon Kim[1,2], Dong Il Park[1]*, Jong-Woo Park[1], Hwi-Su Kim[1], Youngsoo Cho[1], Won-Suk Jung[2]*

[1]Department of Robotics and Mechatronics, Korea Institute of Machinery & Materials (KIMM), Daejeon, Republic of Korea

[2]School of Mechanical Engineering, Chungnam National University (CNU), Daejeon, Republic of Korea

***Corresponding author:** Dong Il Park, parkstar@kimm.re.kr; Won-Suk Jung, wonsuk81@cnu.ac.kr

Abstract

Recently, interest in a dual-arm robot that can replace humans is increasing to improve the working environment and solve the labor shortage. Various studies related to the design and analysis of dual-arm robots have been conducted because dual-arm robots can have various kinematic configurations according to the objective task. It is necessary to evaluate the work performance according to various kinematic structures of the dual arm robot to maximize its effectiveness. In the paper, the performance analysis is studied according to the shoulder configuration and the wrist configuration of the dual-arm robot by using main performance indices such as manipulability, condition number, and minimum singular value by assigning proper weight values to each objective motion. Performance analysis for the robotic assembly process is effectively carried out for each representative dual-arm robot configuration.

Keywords

Dual-arm robot
Robotic assembly
Manipulability analysis
Performance analysis
Kinematic configuration

1. Introduction

To maximize the performance of a robot performing a given task, optimization of design variables and structure based on systematic performance analysis is a very important issue. Therefore, there have been many studies on metrics that can measure the performance of robots under various conditions. The concept of manipulability of representative robots was first introduced by Yoshikawa, who defined manipulability indices including manipulability ellipsoids by mapping joint velocities to end-effector velocity space [1]. Since then, various manipulability studies have been conducted to analyze the performance of different robot configurations [2-6], including a study on algorithms to generate optimal trajectories using the proposed manipulability index [7], and an application study to reconfigure robot links based on manipulability when the target task of the end-effector is fixed [8]. In addition to the kinematic manipulability evaluation and application studies of robots, we have also introduced dynamic performance evaluation of end-effector velocity as well as acceleration and force capability and extended it to analytical studies of acceleration and force capability [9]. There have also been studies on stiffness ellipsoids for determining robot posture and control parameters, and related studies on analyzing the force/deformation behavior of extremities [10,11]. More recently, research has been conducted on analyzing the performance of robots for various dynamic tasks by applying a weighting matrix to the dynamic manipulability index of the robot [12].

Research on human-like dual-arm robots is increasing to perform efficient tasks [13], and since the performance of dual-arm robots varies greatly depending on the shape of the robot, it is essential to evaluate the performance for the intended task. Various analyses have been conducted, ranging from basic theories on the manipulability of dual-arm robots [14] to studies that calculate the manipulability index for each arm posture [15], studies on dexterity evaluation methods such as condition number, determinant, and minimum singular value for manipulators with slack [16], and studies that apply slack to the manipulability index [17]. In addition, there have been studies analyzing common workspace, degrees of freedom, and two-arm manipulability, and studies analyzing the attachment angle of two-arm robots based on two-arm robot manipulability [18].

However, to date, there has been no study that has conducted a systematic performance evaluation that appropriately reflects the requirements for different types of tasks, including the overall structure of the dual-arm robot, such as the shoulder configuration and wrist configuration. In this paper, we propose a methodology to systematically analyze the structure of a dual-arm robot suitable for the assembly process by using major performance indices such as Manipulability, Condition Number, and Minimum Specific Value to derive performance figures for each motion of the two arms, and then introducing a normalization technique and a weighting technique for each motion feature. In this paper, Rethink Robotics' Baxter, ABB's YuMi, and Korea Institute of Machinery Research's Amiro2, which are representative dual-arm robots with seven axes, are used as example robots for comparative analysis [19-21].

Section 2 describes the manipulability evaluation theory to be applied to the evaluation of dual-arm robots, and Section 3 presents the design of the manipulability evaluation process and the motion analysis of the actual assembly process. In Section 4, we apply the proposed methodology to evaluate the manipulability of the target motion and discuss the results and the validity of the proposed methodology.

2. Manipulability assessment theory

2.1. Manipulability index, ellipsoid

The manipulability index is used to determine the range of possible actions for the robot's next behavior. This index, defined by Yoshikawa, is the magnitude of how much the robot's tip wants to move or rotate to the next point. This manipulability index is given by Equation (1).

$$M(\theta) = \sqrt{\det\left(J(\theta)J^T(\theta)\right)} \tag{1}$$

Here, θ is the joint variable, $M(\theta)$ is the manipulability index, and $J(\theta)$ is the Jacobian matrix. If we map the joint velocity from the manipulability index to a circle, we can derive a circle-shaped Cartesian velocity. This is a circular representation of the velocity that can be achieved when progressing from a given posture to the next, as shown in Equation (2).

$$\begin{aligned}\|\dot{\theta}\| &= \sqrt{\dot{\theta}^T\dot{\theta}} = \sqrt{\dot{x}^T(J^\dagger)^T J^\dagger \dot{x}} = \sqrt{\dot{x}^T(JJ^T)^\dagger \dot{x}} \\ &= \sqrt{\dot{x}^T(JJ^T)^{-1}\dot{x}} \le 1\end{aligned} \tag{2}$$

Here, x is the Cartesian variable. This allows eigenvalues and eigenvectors to be defined for each robot posture, as shown in **Figure 1**, and provides a visual representation of the magnitude and direction of the robot's velocity. The larger the eigenvalue corresponding to each eigenvector, the larger the size of the ellipsoid can be, which increases the ratio of the action radius of the robot's end, which can be considered to increase manipulability.

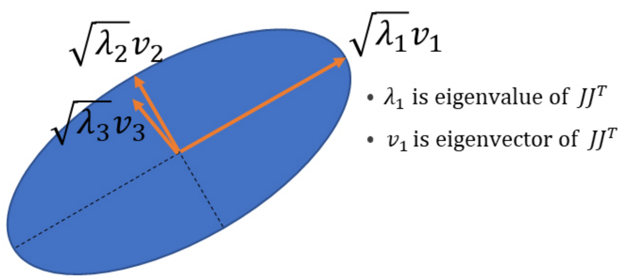

Figure 1. Manipulability ellipsoid

In addition, the velocity manipulability ellipsoid can be used to derive the magnitude and direction of the force in the current posture, which is expressed as the reciprocal of the velocity manipulability ellipsoid, as shown in Equation (3). Here, τ is the joint torque, and f is the fore on the end-effector. If the eigenvalues and eigenvectors are obtained in the same way, it can be seen from $(JJ^T)^{-1}$ and JJ^T that the direction is the same and the magnitude has an inverse, and it can be defined as a force manipulation ellipsoid.

$$\|\tau\| = \sqrt{\tau^T\tau} = \sqrt{f^T(JJ^T)f} \leq 1 \tag{3}$$

2.2. Minimum singular value

The minimum singular value is the value with the lowest action radius ratio in the current posture, as shown in **Figure 2**. The maximum value of the joint velocity is limited by the minimum singular value ($\sqrt{\lambda_m}$) as shown in Equation (4).

$$\|\dot{\theta}\| \leq (\frac{1}{\sqrt{\lambda_m}})\|\dot{x}\| \tag{4}$$

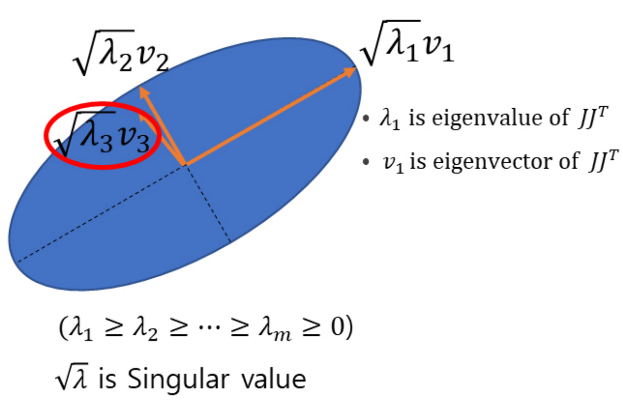

Figure 2. Minimum singular value

2.3. Condition number

The condition number is used to evaluate the uniformity of the manipulability ellipsoid represented by the robot's current posture. The definition of the condition number studied by Salisbury and Craig is expressed as the ratio of the minimum and maximum characteristic values as shown in **Figure 3**, which shows the degree of uniformity of the action radius from the current posture to the next posture. Under the assumption that the maximum characteristic value is constant, the greater the degree of uniformity, the greater the ratio of the action radius, so it can be seen that the manipulability increases, and the expression of the condition index is as follows:

$$Condition\ number\ (k) = \frac{\sqrt{\lambda_1}}{\sqrt{\lambda_m}} \tag{5}$$

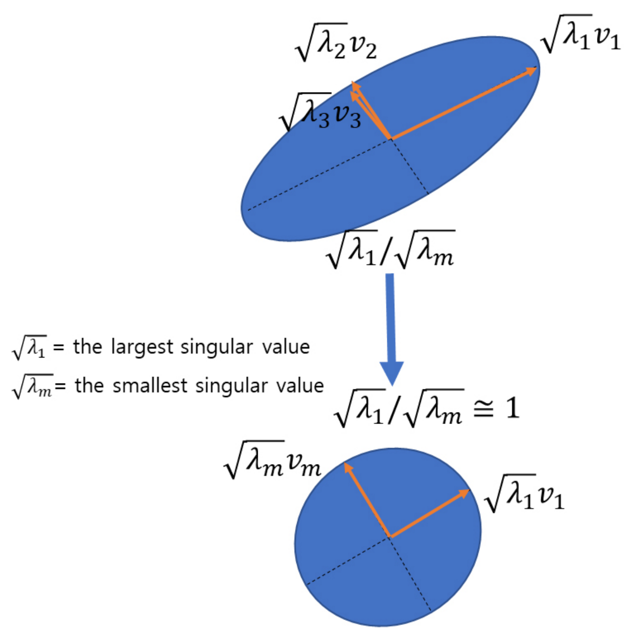

Figure 3. Condition number

3. Evaluation of manipulability for dual-arm robots

3.1. Design of evaluation methods

In this paper, a simulation using MATLAB was performed to analyze the behavior of the dual-arm robot. Various performance indexes introduced above were fused to evaluate the task performance of the dual-arm robot according to its structure.

$$\begin{bmatrix} F_{P.1} \\ \vdots \\ F_{P.n} \end{bmatrix} = \begin{bmatrix} W_{11} & \cdots & W_{14} \\ \vdots & \ddots & \vdots \\ W_{n1} & \cdots & W_{n4} \end{bmatrix} \begin{bmatrix} f_{vel.e} \\ f_{min} \\ f_{cond} \\ f_{force.e} \end{bmatrix} \tag{6}$$

Here, W_{11}~W_{n4} is the weighting value for each index and motion. $F_{P.1},\ldots, F_{P.n}$ refers to the composite performance index in each posture corresponding to postures 1 to n among the total tasks of the dual-arm robot, and the number of n can be expanded according to the motion and further expanded if it is necessary to distinguish between the tasks of the left and right arms. f_{vele} is the speed manipulability index which follows Equations (1) and (2), f_{min} is the minimum specific value from Equation (4), f_{cond} is the state index from Equation (5), and $f_{force,e}$ is the force manipulability index which is calculated from Equation (3).

The evaluation of the overall performance index is given by Equation (6), and the calculation procedure is as follows. Firstly, the target task to be performed by the dual-arm robot is classified into distinct actions, and the weight of the performance index is selected for each classified action to suit the task goal. Secondly, calculate the value of each performance index for the target task. Thirdly, the calculated indices are mapped to a 0 to 1 value by applying a min-max normalization method to adjust their sensitivity. Finally, the value with the largest sum is applied to Equation (7) to evaluate the best robot for the target task.

$$Total\ performance = \sum_{i=1}^{n} F_{P.i} \tag{7}$$

3.2. Definition of motions

To validate the performance evaluation process of the dual-arm robot, we defined the motion shown in **Figure 4** as an example of the camera rewind wheel part used in the cell assembly process. The specific motion has the task sequence of picking up the part from the assembly table, digging the part with the left arm, and tightening the bolt with the right arm, as shown in **Figure 5**.

Figure 5(a) shows the initial position of the dual-arm robot. The motion from Figure **5(b)** to **(c)** is defined as picking up the part from the work table. This motion is defined as "Case 1". The motion in **Figure 5(d)** is the motion of lifting the part to prepare it for assembly and is defined as "Case 2". Lastly, the motion from **Figure 5(e)** to **(f)** is to grip the part and perform bolt tightening by giving it a rotational motion to fully utilize the characteristics of the wrist structure, which is defined as "Case 3".

(a)

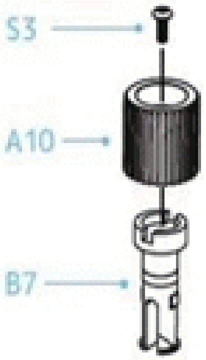

(b)

Figure 4. (a) Assembling rewind wheel; **(b)** Rewind wheel

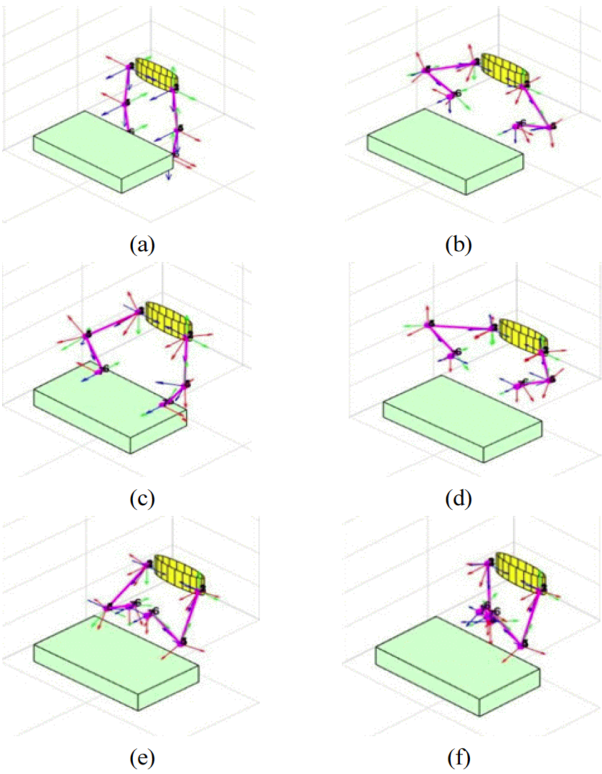

Figure 5. Assembling motion for rewind wheel

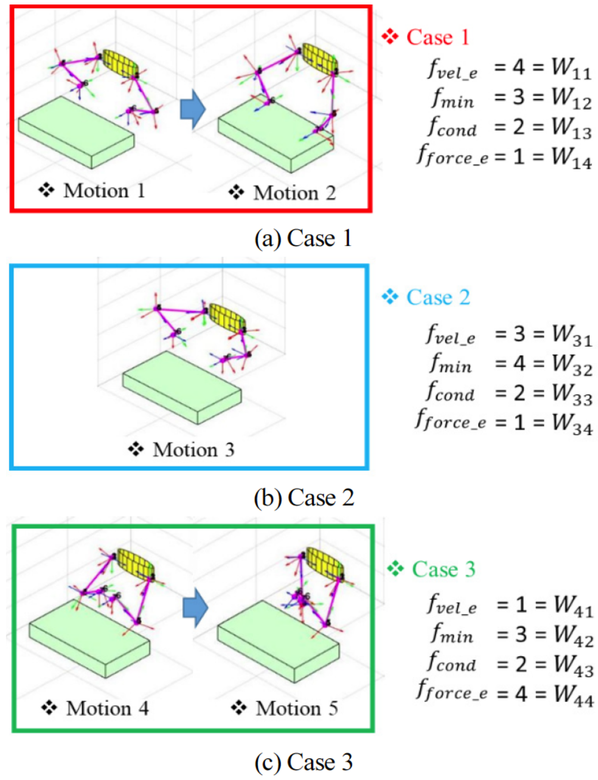

Figure 6. Separated motion cases

The reason for dividing into various cases is that each motion has a different purpose and a different weight of manipulability, and the weight of each case is distributed based on the sum of 10, and the weighting result of each case is shown in **Figure 6**.

In "Case 1", since it is a motion to go to the work table for gripping parts, the operability index was given a large weight of 4, and the minimum specific value was given a weight of 3. In "Case 2", since the main purpose is to select the assembly location, the minimum specificity value is 4 and the operability index is 3, giving more weight to the direction of movement. Both "Case 1" and "Case 2" can be considered as similar cases with similar weights because they are moving for assembly preparation and the only difference is the direction. In "Case 3", the main purpose of the motion is assembly, so the force manipulability index is given the highest weight, which is an example of weighting to reflect the characteristics of the purposeful motion.

The important point here is that the value of the weight is not the only one that is fixed at a certain value, but the user can freely change the weight to evaluate the performance by comprehensively considering the type of target task, the importance of each motion of the target task, the direction of the task, the speed of the task, and the force of the task, and the main feature is that the proposed technique can be applied freely.

3.3. Min-max normalization

The performance indices measured in the assembly process have been previously summarized and normalized to evaluate them on the same basis. The normalization method used is min-max normalization, which normalizes the values of the measured performance indexes to a value between 0 and 1. By mapping the values, it is possible to evaluate performance indices with different values on the same basis. The min-max normalization method was performed using Equation (8).

$$x_s = \frac{x - x_{min}}{x_{max} - x_{min}} \tag{8}$$

Here, x_s is the normalized value of all measured performance indexes for each structure of the dual-arm robot in the assembly process.

3.4. Definition of dual-arm robot structures

Three shoulder structures and three wrist structures were defined to derive the most optimized deal-arm structure for the target task. We adopted Baxter, Yumi, and Amiro2 (Human structure) from the Korea Institute of Machinery Research, which have different structures among industrial dual-arm robots, as shown in **Figure 7**. Baxter's shoulder structure has a unique shape, and Yumi and Amiro2 have similar structures, but differences exist in the directional angle at which the shoulder is attached.

In addition to the shoulder structure, the wrist structure also affects the work, so we classified the most representative wrist structures in industrial robotic arms, ZYZ, ZYX, and XYZ structures, as shown in **Figure 8**, and combined them with the shoulder structures of the three robots mentioned above, Baxter, Yumi, and Amiro2, to form a total of nine different robot structures.

Since the robots utilized in this process all have 7DOF per arm, they do not have a single joint solution for the same objective task. However, the energy optimization solution, which is the minimum norm solution, is applied in this paper to analyze each robot system under the same conditions.

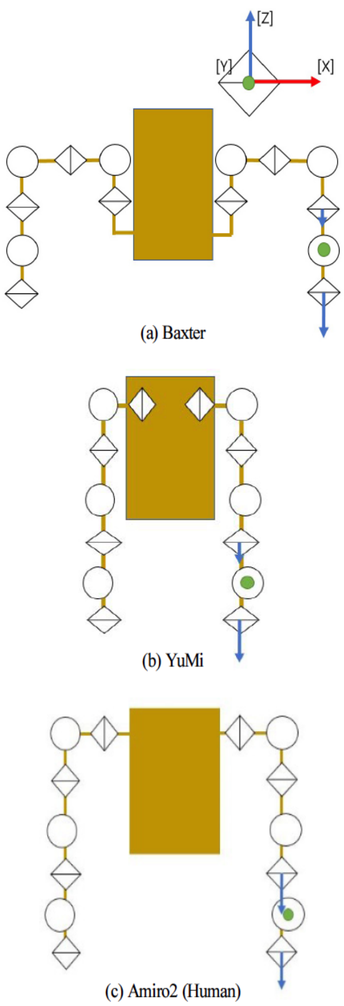

Figure 7. Three types of shoulder configuration

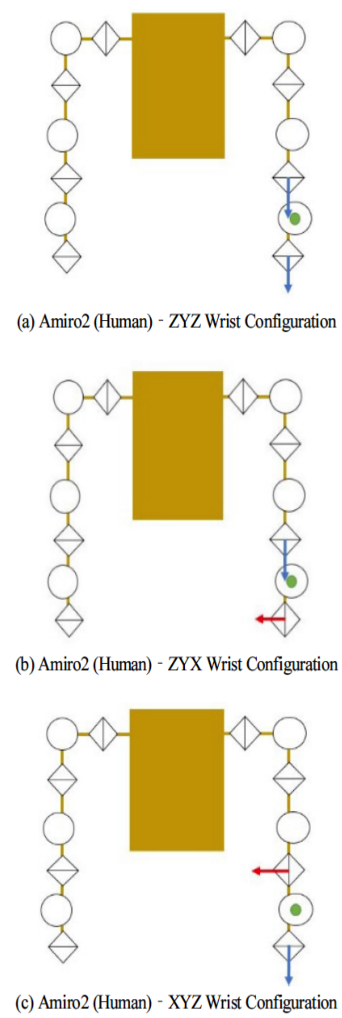

Figure 8. Three types of wrist configuration

4. Manipulability assessment and discussion

4.1. Evaluation of simulation motions for dual-arm robots

The result of the task analysis for the Amiro2-ZYZ structure using the MATLAB simulation introduced earlier is shown in **Figure 9**.

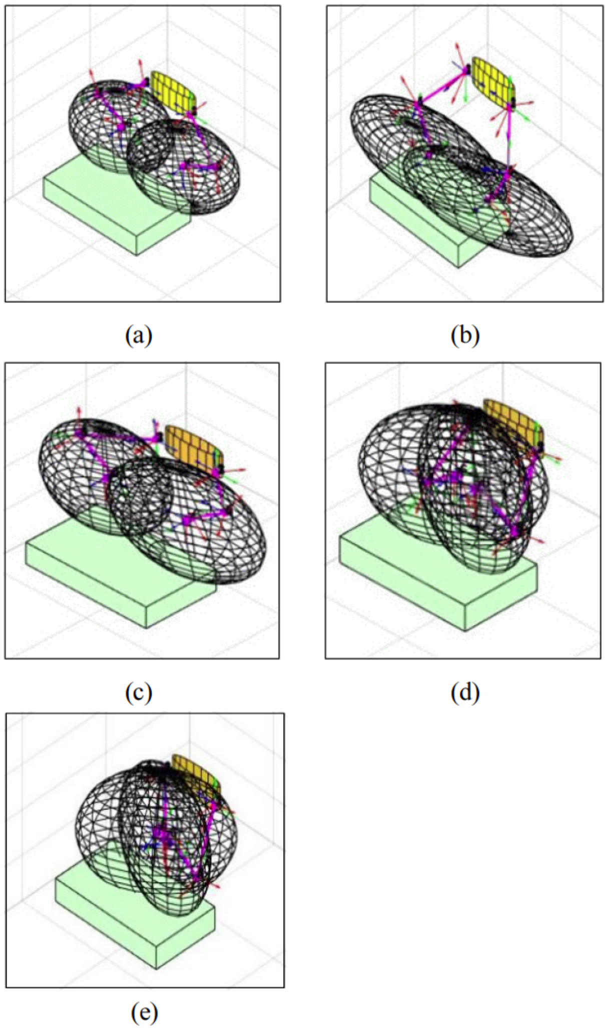

Figure 9. Motion simulation, manipulability ellipsoid

4.2. Performance index evaluation for motions of Amiro, Baxter, and YuMi structures

We measured the performance indexes of the dual-arm robots for each motion and performed a comparative evaluation. Before mapping the indexes for evaluation, **Figure 10** shows the measured values of Amiro2 - ZYZ, ZYX, and XYZ structures and mapped with min-max normalization.

The manipulability ellipsoid (normV) is an indicator of the ability to move a larger range from the current posture, with the highest values representing good manipulability. Based on the values we measured, the ZYZ wrist structure has the best overall motion. However, this is based on the size of the ellipsoid alone, so we cannot predict how it will behave [22]. By comparing the minimum singularity value (normM) of each motion, we can evaluate the weakest orientation that the robot can have in its current posture, i.e., the orientation and size close to the singularity. By comparing the state index (normC) for each motion, the shape of the ellipsoid can be determined. This tells us how close the ellipsoid is to the singularity and how much motion there is in the free range. By comparing the manipulability ellipsoid (normF) of the force of each motion, we can evaluate the magnitude and direction of the force that the robot can exert in its current posture. Due to equation (3), the size is the same as the manipulability ellipsoid we compared earlier, but it is reciprocal, so the shape of the ellipsoid is orthogonal. This means that the direction of the minimum value in the manipulability ellipsoid is the direction of the maximum value in the force manipulability ellipsoid.

When analyzing the performance index for the same motion as the assembly process task applied to the Amiro2 (Human) rescue robot earlier, the performance index for the Baxter-type robot is shown in **Figure 11** and the YuMi-type robot is shown in **Figure 12**. Here, the blank area indicates the work area that cannot be performed with the structure.

4.3. Discussion of manipulability results for dual-arm robots in specific tasks

The performance indexes measured in the assembly process, which were normalized earlier, and the selected weights for each motion are applied to the proposed evaluation model equation (8), and the

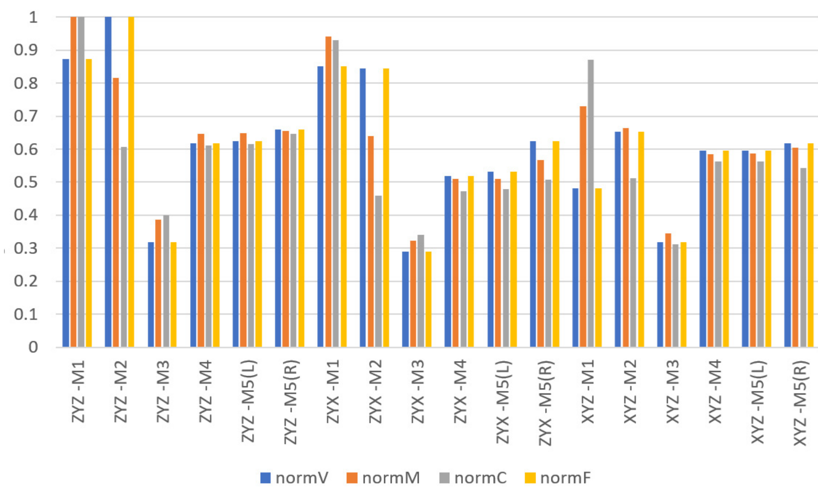

Figure 10. Amiro2 (Human) – ZYZ, ZYX, XYZ configuration

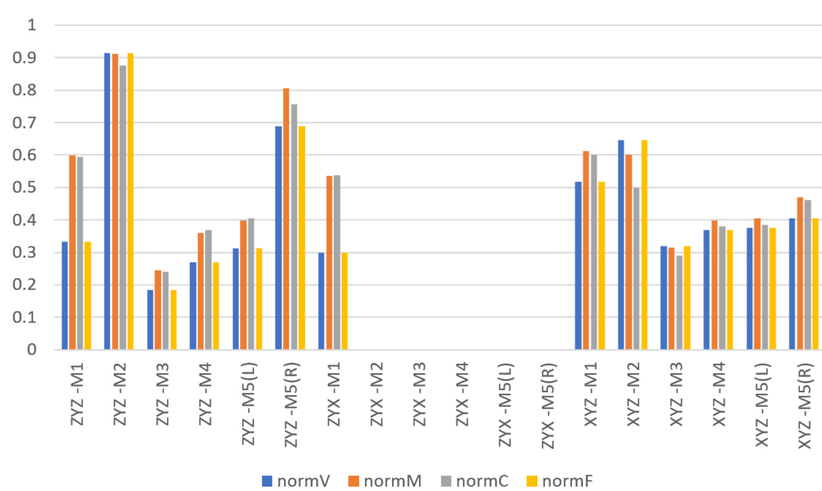

Figure 11. Baxter – ZYZ, ZYX, XYZ configuration

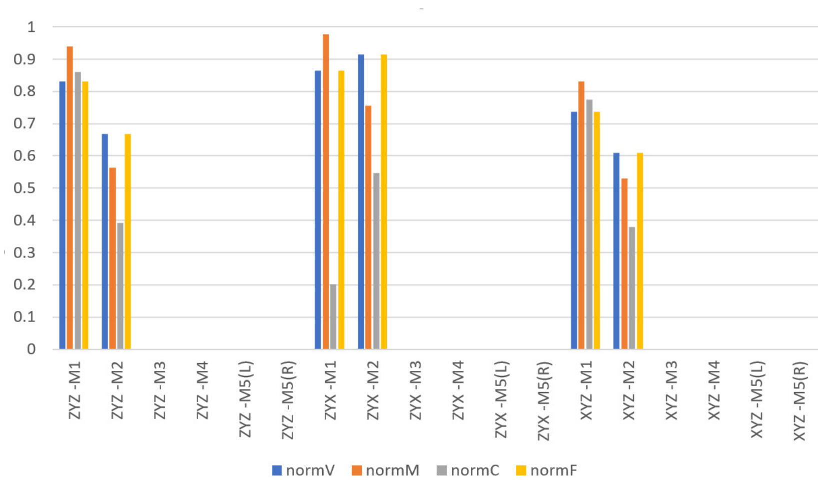

Figure 12. YuMi – ZYZ, ZYX, XYZ configuration

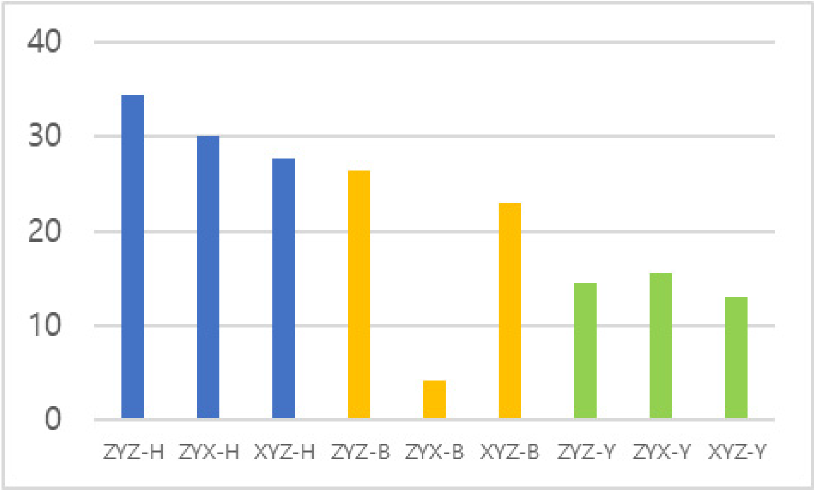

Figure 13. Configuration evaluation

weights are applied with the values selected in **Figure 6**.

A total sum is calculated by applying weights to the performance indexes for each motion, and the larger the value of the total sum, the more optimized the robot is for the target task of the dual-arm robot. The evaluated values for each structure were derived as shown in **Figure 13**.

As a result of the evaluation of the overall performance index for the target task extracted from the camera component assembly process, it was found that the Amiro-ZYZ structure has relatively high manipulability for the target motions. However, this is an example of a result that indicates that a robot structure that is specific to a particular task may be more appropriate. The motions evaluated in this study are suitable for specific purposes, such as performing dual-arm orthogonal assembly tasks, with high weighting on speed in "Case 1", directional weighting in "Case 2", and high weighting on force manipulation in "Case 3".

In addition to these cases, whenever conditions such as the target work area, work speed, and workforce are changed, or the weighting of each target value is changed accordingly, the task performance of each structure can be predicted through this process, and solutions of various structures can be derived.

5. Conclusion

In this paper, we proposed a systematic method for measuring and evaluating the manipulability of dual-arm robots according to their structural characteristics, using the measurement methods of previously researched robots. We derived representative motions based on the desired tasks, performed a performance evaluation of various dual-arm robot structures by selecting weights for each motion based on their objectives, and identified the suitable form of dual-arm robots for the selected tasks and conditions. Based on this manipulability evaluation method presented in this paper, it will be possible to systematically evaluate various tasks and structures beyond the motions and dual-arm robot structures proposed in this study. In future research, we intend to expand the scope of manipulability assessment by considering kinematic elements and the relative motion of dual-arm robots.

Disclosure statement

The authors declare no conflict of interest.

Funding

This project is currently supported by the Technology Innovation Program (No. 1415169457) funded by the Ministry of Trade, Industry, and Energy, Korea Government.

References

[1] Yoshikawa T, 1985, Manipulability of Robotic Mechanisms. The International Journal of Robotics Research, 4(2): 3 – 9. https://doi.org/10.1177/027836498500400201

[2] Staffetti E, Bruyninck H, De Schutter J. On the Invariance of Manipulability Indices. In Advances in Robot Kinematics: Theory and Applications. 2002, Springer, 57–66. https://doi.org/10.1007/978-94-017-0657-5

[3] Salisbury JK, Craig JJ, 1982, Articulated Hands: Force Control and Kinematic Issues. The International Journal of Robotics Research, 1(1): 4–17. https://doi.org/10.1177/027836498200100102

[4] Kim J-O, Khosla K. IROS '91: IEEE/RSJ International Workshop on Intelligent Robots and Systems, November 3–5, 1991: Dexterity Measures for Design and Control of Manipulators. 1991, Osaka, 756–763. https://doi.org/10.1109/IROS.1991.174572

[5] Chiu SL. 1988 IEEE International Conference on Robotics and Automation, April 24–29, 1988: Kinematic Characterization of Manipulators: An Approach to Defining Optimality. 1988, Philadelphia, 828–833. https://doi.org/10.1109/ROBOT.1988.12163

[6] Angeles J, López-Cajún CS, 1992, Kinematic Isotropy and the Conditioning Index of Serial Robotic Manipulators. The International Journal of Robotics Research, 11(6): 560–571. https://doi.org/10.1177/027836499201100605

[7] Guilamo L, Kuffner J, Nishiwaki K, et al. 2006 IEEE International Conference on Robotics and Automation, May 15–19, 2006: Manipulability Optimization for Trajectory Generation. 2006, Orlando, 2017–2022. https://doi.org/10.1109/ROBOT.2006.1642001

[8] Zhang T, Minami M, Yasukura O, et al., 2013, Reconfiguration Manipulability Analyses for Redundant Robots. ASME Journal of Mechanisms Robotics, 5(4): 041001. https://doi.org/10.1115/1.4024727

[9] Bowling A, Khatib O, 2005, The Dynamic Capability Equations: A New Tool for Analyzing Robotic Manipulator Performance. IEEE Transactions on Robotics, 21(1): 115–123. https://doi.org/10.1109/TRO.2004.837243

[10] Ajoudani A, Tsagarakis NG, Bicchi A. 2015 IEEE International Conference on Robotics and Automation (ICRA), May 26–30, 2015: On the Role of Robot Configuration in Cartesian Stiffness Control. 2015, Seattle, 1010–1016. https://doi.org/10.1109/ICRA.2015.7139300

[11] Ajoudani A, Tsagarakis NG, Bicchi A, 2017, Choosing Poses for Force and Stiffness Control. IEEE Transactions on Robotics, 33(6): 1483–1490. https://doi.org/10.1109/TRO.2017.2708087

[12] Azad M, Babič J, Mistry M, 2019, Effects of the Weighting Matrix on Dynamic Manipulability of Robots. Autonomous Robots, 43: 1867–1879. https://doi.org/10.1007/s10514-018-09819-y

[13] Smith C, Karayiannidis Y, Nalpantidis L, et al., 2012, Dual Arm Manipulation – A Survey. Robotics and Autonomous Systems, 60(10): 1340–1353. https://doi.org/10.1016/j.robot.2012.07.005

[14] Lee S, 1989, Dual Redundant Arm Configuration Optimization with Task-Oriented Dual Arm Manipulability. IEEE Transactions on Robotics and Automation, 5(1): 78–97. https://doi.org/10.1109/70.88020

[15] Choi M-H, Lee M-Y, Lee B-H, et al., 1990, On the Manipulability Measure of Dual Arm. Institute of Control, Robotics and Systems, 1990: 1156–1161. https://www.koreascience.or.kr/article/CFKO199011919696004.page.

[16] Klein CA, Blaho BE, 1987, Dexterity Measures for the Design and Control of Kinematically Redundant Manipulators. The International Journal of Robotics Research, 6(2): 72–83. https://doi.org/10.1177/027836498700600206

[17] Vahrenkamp N, Asfour T, Metta G, et al. 2012 12th IEEE-RAS International Conference on Humanoid Robots (Humanoids 2012), November 29–December 1, 2012: Manipulability Analysis. 2012, Osaka, 568–573. https://doi.org/10.1109/HUMANOIDS.2012.6651576

[18] Bagheri M, Ajoudani A, Lee J, et al. 2015 IEEE International Conference on Robotics and Automation (ICRA), May 26–30, 2015: Kinematic Analysis and Design Considerations for Optimal Base Frame Arrangement of Humanoid Shoulders. 2015, Seattle, 2710–2715. https://doi.org/10.1109/ICRA.2015.7139566

[19] Ju Z, Yang C, Ma H. Proceedings of the 33rd Chinese Control Conference, July 28–30, 2014: Kinematics Modeling and Experimental Verification of Baxter Robot. 2014, Nanjing, 8518–8523. https://doi.org/10.1109/ChiCC.2014.6896430

[20] Kirgis F-P, Katsos P, Kohlmaier M. Collaborative Robotics. In Robotic Fabrication in Architecture, Art and Design. 2016, Springer Int, Switzerland, 448–453. https://doi.org/10.1007/978-3-319-26378-6

[21] Park DI, Park C, Do H, et al. 2014 14th International Conference on Control, Automation and Systems (ICCAS 2014), October 22–25, 2014: Development of Dual Arm Robot Platform for Automatic Assembly. 2014, Gyeonggi-do, 319–321. https://doi.org/10.1109/ICCAS.2014.6988013

[22] Gosselin CM, 1992, The Optimum Design of Robotic Manipulators Using Dexterity Indices. Robotics and Autonomous Systems, 9(4): 213–226. https://doi.org/10.1016/0921-8890(92)90039-2

Publisher's note

Art & Technology Publishing remains neutral with regard to jurisdictional claims in published maps and institutional affiliations.